

FORGE

Fate Of Repository Gases

European Commission FP7

FORGE WP2 Progress report

FORGE Report D2.4– VER.0 (February 2013)

	Name	Organisation	Signature	Date
Compiled	D. Stammose A. Vokal	IRSN (France) NRI (Czech Rep.)		18/02/2013
Verified	D. Pellegrini	IRSN (France)		25/02/2013
Approved	R. Shaw	NERC BGS (UK)		29 November 2013

Keywords

Hydrogen generation,
corrosion, carbon steel,
bentonite, Irradiation.

Bibliographical reference

Stammose, D., Vokal, A.. 2013.
FORGE WP2 - Progress report.
FORGE Report D2.4. 31pp.

Euratom 7th Framework Programme Project: FORGE



Fate of repository gases (FORGE)

The multiple barrier concept is the cornerstone of all proposed schemes for underground disposal of radioactive wastes. The concept invokes a series of barriers, both engineered and natural, between the waste and the surface. Achieving this concept is the primary objective of all disposal programmes, from site appraisal and characterisation to repository design and construction. However, the performance of the repository as a whole (waste, buffer, engineering disturbed zone, host rock), and in particular its gas transport properties, are still poorly understood. Issues still to be adequately examined that relate to understanding basic processes include: dilational versus visco-capillary flow mechanisms; long-term integrity of seals, in particular gas flow along contacts; role of the EDZ as a conduit for preferential flow; laboratory to field up-scaling. Understanding gas generation and migration is thus vital in the quantitative assessment of repositories and is the focus of the research in this integrated, multi-disciplinary project. The FORGE project is a pan-European project with links to international radioactive waste management organisations, regulators and academia, specifically designed to tackle the key research issues associated with the generation and movement of repository gasses. Of particular importance are the long-term performance of bentonite buffers, plastic clays, indurated mudrocks and crystalline formations. Further experimental data are required to reduce uncertainty relating to the quantitative treatment of gas in performance assessment. FORGE will address these issues through a series of laboratory and field-scale experiments, including the development of new methods for up-scaling allowing the optimisation of concepts through detailed scenario analysis. The FORGE partners are committed to training and CPD through a broad portfolio of training opportunities and initiatives which form a significant part of the project.

Further details on the FORGE project and its outcomes can be accessed at www.FORGEproject.org.

Contact details:

EC FORGE Work Package 2 Leader:

Dr Delphine PELLEGRINI

Organisation: IRSN

Tel: 33 (1) 58 35 74 53

Fax 33 (1) 58 35 79 76

email: delphine.pellegrini@irsn.fr

web address: www.irsn.fr

Address: 31 avenue de la Division Leclerc

92260 Fontenay aux Roses Cedex

FRANCE

..

Acknowledgements

Of the many individuals who have contributed to the project, the authors would particularly like to thank the following:

Mr P. POLIVKA from NRI (Czech Republic)

Mr D. DOBREV from NRI (Czech Republic)

Mr B. MARCILLAUD from IRSN/PSN-RES/SCA/LPMA (France)

Dr L. BERGER from IRSN/PSN-RES/SCA/BIREN (France)

Mr M. RABOIN from IRSN/PSN-RES/SCA/BIREN (France)

Contents

Acknowledgements	2
Contents.....	3
Summary	6
1 NRI Experiments.....	7
1.1 Experimental method.....	7
1.2 Preliminary results from long term experiment with hydrogen generation	9
1.3 Hydrogen migration through compacted bentonite.....	11
1.3.1 Introduction.....	11
1.3.2 Experimental method.....	11
1.3.3 Results and Discussion	14
1.4 Conclusions.....	21
2 IRSN Experiments.....	22
2.1 Experimental method.....	22
2.2 Results	23
2.3 Discussion	25
2.4 Conclusions.....	29
References.....	31

List of Figures

Fig. 1: The corrosion chamber for measuring hydrogen evolution under radiation before modification	8
Fig. 2: Hydrogen evolution from anaerobic corrosion of carbon steel cylinder at 80 °C in anaerobic box.....	9
Fig. 3: Hydrogen evolution rate from long-term experiment conducted at 80 °C in an anaerobic box.....	10
Fig. 4: Results of measuring Eh and pH of the solution	10
Fig. 5: Scheme of device for measuring hydrogen migration without backpressure	13
Fig. 6: Scheme of device for measuring hydrogen migration with backpressure from compression machine	13
Fig. 7: Device for measuring hydrogen migration from a hydrogen reservoir under constant pressure (P – pump, W –plexi window, NT – needle valve, V – volume gauge).....	14
Fig. 8: Hydrogen breakthrough pressure curves for samples of bentonite Rokle of various densities	15
Fig. 9: Breakthrough curve for bentonite Rokle of density 1600 kg/m ³	15
Fig. 10: Breakthrough curve for Wyoming type bentonite (Volclay KWK-20-80) with dry density 1600 g/cm ³	16
Fig. 11: Breakthrough curve for MX-80 bentonite (1600 kg/m ³)	16
Fig. 12: Change of pressure and volume due to release of hydrogen for Wyoming type (Volclay KWK-20-80) bentonite before the first breakthrough	17
Fig. 13: Change of pressure and volume due to release of hydrogen for Rokle type bentonite before the first breakthrough	17
Fig. 14: Pressure and volume increase of Volclay bentonite from Voltex waterproofing system due hydrogen generation	19
Fig. 15: Pressure and volume change due to hydrogen transport in bentonite Rokle 75 (before the first breakthrough).....	20
Fig. 16: Pressure and volume change after the first breakthrough in Rokle 75	20
Fig. 17: Hydrogen flow through compacted, saturated bentonite (Rokle) at hydrogen pressure of 8 MPa	21
Fig. 18: Experimental device	22
Fig. 19: Steps of an experiment.....	23

Fig. 20: Hydrogen release versus time $M_{Fe} = 10 \text{ g}$, $V_{H_2O} = 100 \text{ ml}$ – dose rate = 100 Gy/h..... 24

Fig. 21: Hydrogen release versus time $M_{Fe} = 10 \text{ g}$, $V_{H_2O} = 100 \text{ ml}$ – dose rate = 50 Gy/h 25

Fig. 22: Hydrogen production rate (mol/min) versus time (min)..... 26

Fig. 23: Hydrogen production rate (mol/min) versus time (min) – Corrected from water radiolysis contribution. 28

List of Tables

Table 1: Composition of carbon steel 7

Table 2: Compositions and chemicals for preparation of synthetic bentonite water..... 7

Table 3: Mineralogical composition of tested bentonites 12

Table 4: Hydraulic conductivities of bentonites..... 12

Table 5: Solution analysis 25

Table 6: H_2 production rate during step 1 for the two experiments 26

Table 7: Allen chain 27

Table 8: Hydrogen production by water radiolysis in mol/min 28

Summary

This report presents the experimental progress made by the two partners involved in Work Package 2 on hydrogen generation from corrosion of carbon steel and iron.

The experiments carried out by NRI were focused in this period on conducting long-term experiment with gas generation from anaerobic corrosion of carbon steel in an anaerobic box and studying migration of hydrogen through compacted bentonite. The long-term experiment on hydrogen generation conducted in an anaerobic box is still under way so that only preliminary results are presented in this progress report.

IRSN has carried out irradiation experiments at 2 dose rates (100 and 50 Gy/h) using the new device developed during the previous year. Hydrogen production was monitored through continuous measurements during all the duration of the experiments (at least 4 weeks). According to the results obtained, it seems that irradiation (at these dose rates) influences corrosion processes and induces an enhancement of hydrogen production. However, this preliminary observation has to be further supported by additional data.

1 NRI Experiments

1.1 EXPERIMENTAL METHOD

The long-term experiment is conducted with carbon steel sample (standard EN 10204/3.1) of cylindrical form (surface 141 cm²). The layer of carbon steel sample affected possibly by atmospheric oxidation or non-uniform surface was removed by lathe before the experiment. The content of impurities in the carbon steel of this standard is given in the following Table 1.

Table 1: Composition of carbon steel

Element	C	P	Mn	S
%	0.1	0.035	0.45	0.035

The composition of synthetic bentonite water and quantity of chemicals used for its preparation is given in the Table 2. The initial pH of this water was 7.5, approximately, conductivity 2100 mS.m⁻¹, and ionic strength 0.29 mol.l⁻¹.

Table 2: Compositions and chemicals for preparation of synthetic bentonite water

Salt	m [g.l ⁻¹]	ion	m [mol.l ⁻¹]
NaCl	0	Na ⁺	0.2
KCl	0.2013	K ⁺	0.0036
MgCl ₂ .6H ₂ O	1.5491	Mg ²⁺	0.0190
MgSO ₄ .2H ₂ O	0.5438	Ca ²⁺	0.0087
CaCl ₂ .2H ₂ O	0	Cl ⁻	0.065
CaSO ₄ .2H ₂ O	1.5842	SO ₄ ²⁻	0.1
SrCl ₂ .6H ₂ O	0.0216	F ⁻	0.0003
Na ₂ SO ₄	12.843	HCO ₃ ⁻	0.0008
NaHCO ₃	0.0748		
NaF	0.0092		

The bentonite water should correspond to the composition of sodium bentonite Volclay KWK 20-80 of a density of 1600 kg.m⁻³.

The hydrogen generation rate was determined by measuring hydrogen evolved from corroding carbon steel using equipment described in our previous reports (Deliverable 2.3). The device enables to measure hydrogen evolution continuously at different temperatures and at a constant pressure in water. The source of pressure is heavy piston, moving in mutually interconnected pressurized cylindrical vessels with a rolling membrane (Brůha and Pelech,

1989). The measurement of volume is based on the detection of the piston position, which depends on the medium volume.

The corrosion experiments are conducted in the device, which scheme is shown in Fig. 2. It uses the same principle of measuring hydrogen generation rate from the volume change with LVDT Displacement Transducer as described above. To seal the device against hydrogen leaking a special sealing system had to be developed.

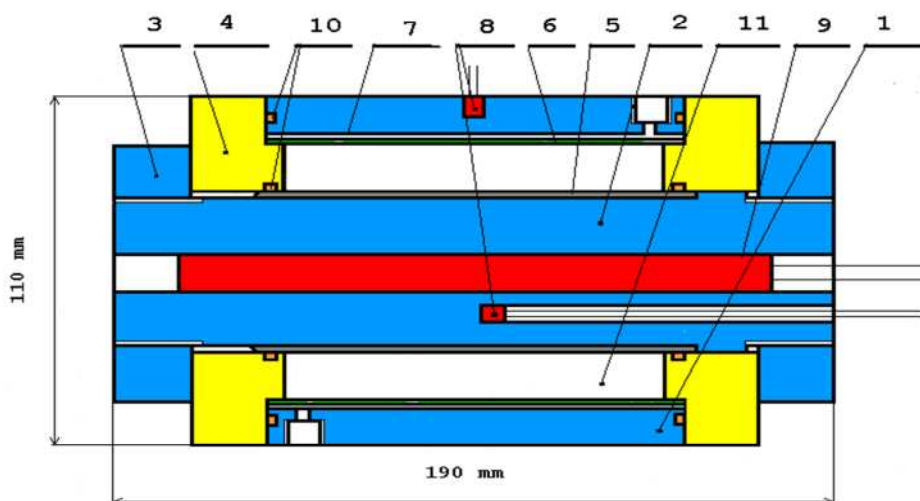


Fig. 1: The corrosion chamber for measuring hydrogen evolution under radiation before modification

1. Chamber case
2. Chamber body
3. Nuts
4. Cover
5. Sample in the form of a tube
6. Filtration textile
7. Watering tube
8. Temperature sensor
9. Heater
10. Sealing O circles
11. Solution, bentonite or other material

Two independent electrodes, platinum wire electrode of diameter 1 mm, length of 20 mm (Beckman Instruments, USA) and gold wire electrode of diameter 1 mm, length 50 mm (Safina, Czech Republic), were used to measure redox potential continuously in the corrosion system with carbon steel and bentonite water. The redox potential was measured between work electrode (platinum, gold) and reference Ag/AgCl electrodes. These reference electrodes were prepared by coating Ag wire by silver chloride in our laboratory. During the experiments working and reference electrodes were cleaned from precipitated corrosion products by hydrochloric acid. Combined platinum electrode ORC 103–BAZ (Theta '90, Czech Republic, platinum disc of diameter 4 mm) was also used to measure Eh in system with steel plates (measuring period 1 day). The same platinum electrode and additional XCL 101 XB2 platinum electrode (Gryf HB, Czech Republic, platinum disc of diameter 2 mm) were used for measuring

the redox potential in the corrosion system with iron powder. For measuring pH HC 113 electrode (Theta '90, Czech Republic) was used and in the system with the iron powder also pH PCL 321 XB2 electrode (Gryf HB, Czech Republic). The electrodes from Gryf HB company were used also for measuring in system with carbon steel wire.

The experiments are carried out in the anaerobic box (MBrown, Germany) with content of oxygen lower than 0.1 ppm. The solution for corrosion was added to the box two weeks before the experiments.

1.2 PRELIMINARY RESULTS FROM LONG TERM EXPERIMENT WITH HYDROGEN GENERATION

The current hydrogen evolution curve from the long-term experiment in the anaerobic box with oxygen content less than 0.1 ppm is shown Fig. 2.

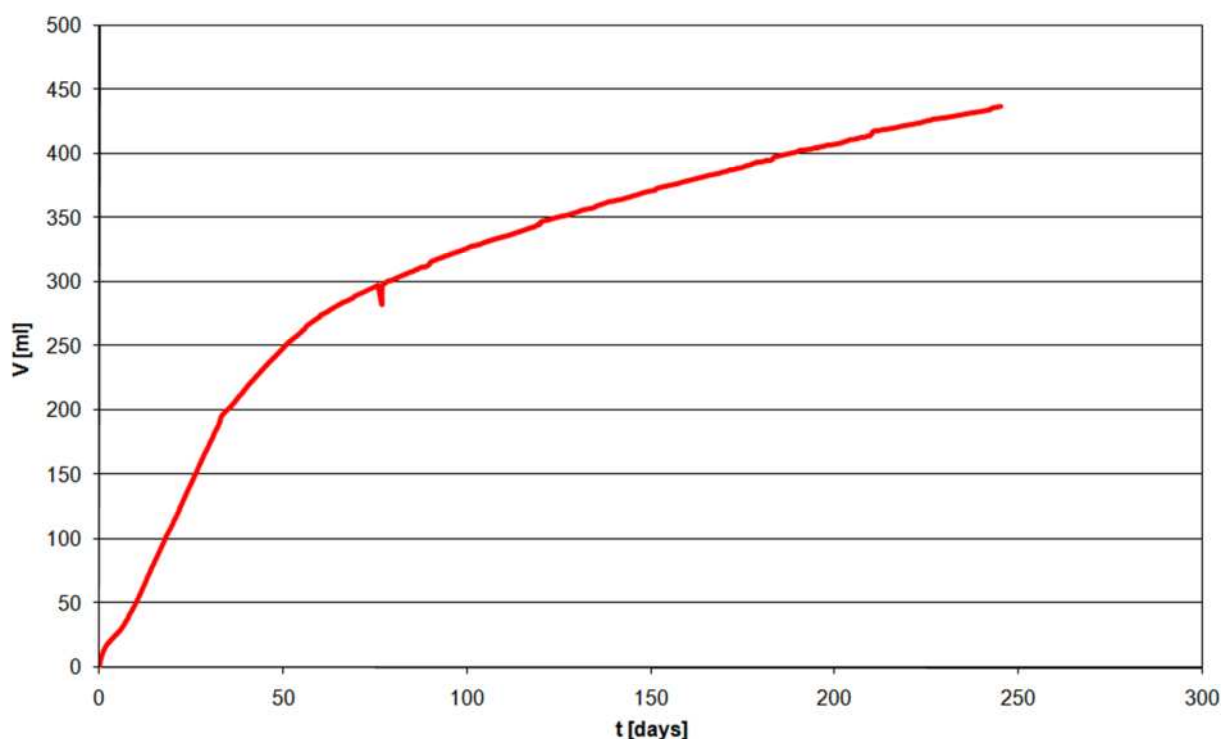


Fig. 2: Hydrogen evolution from anaerobic corrosion of carbon steel cylinder at 80 °C in anaerobic box

The numerical derivation of the curve shown on Fig. 2 recalculated in mol of $\text{H}_2 \text{ m}^{-2} \text{ yr}^{-1}$ is shown in Fig. 3.

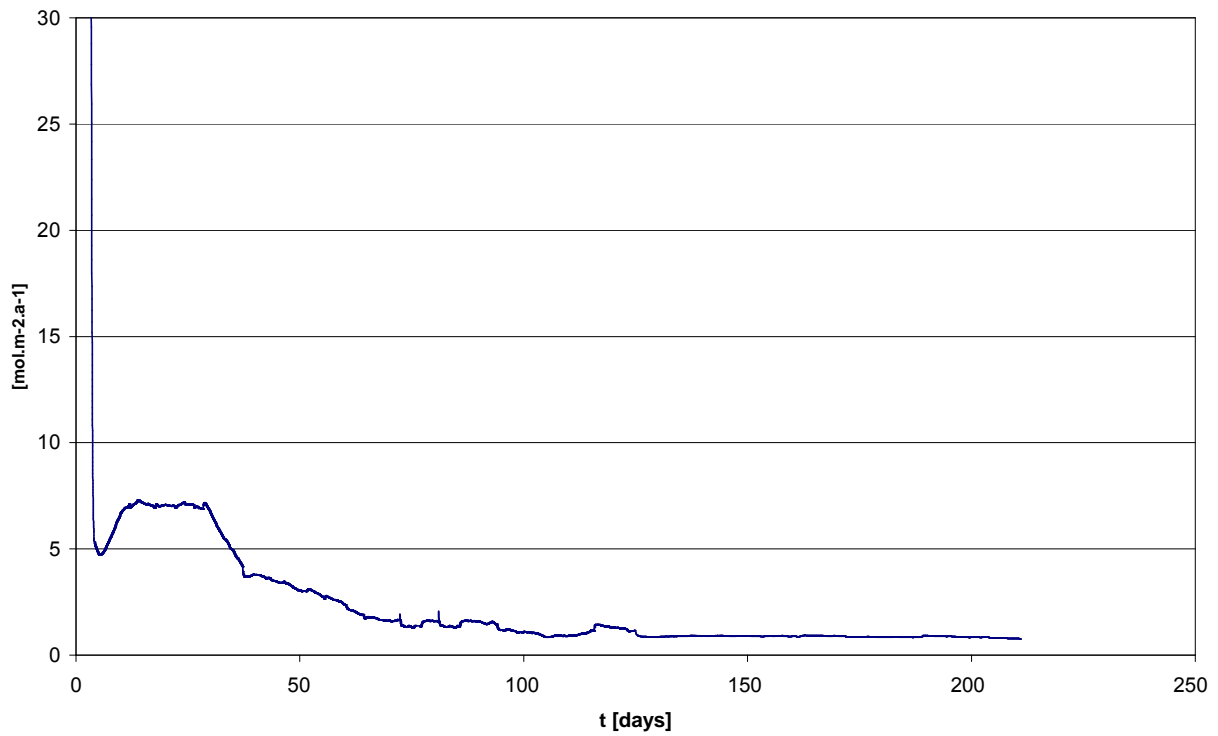


Fig. 3: Hydrogen evolution rate from long-term experiment conducted at 80 °C in an anaerobic box

The results of discontinuous measuring Eh and pH with various types of electrodes are given in Fig. 4.

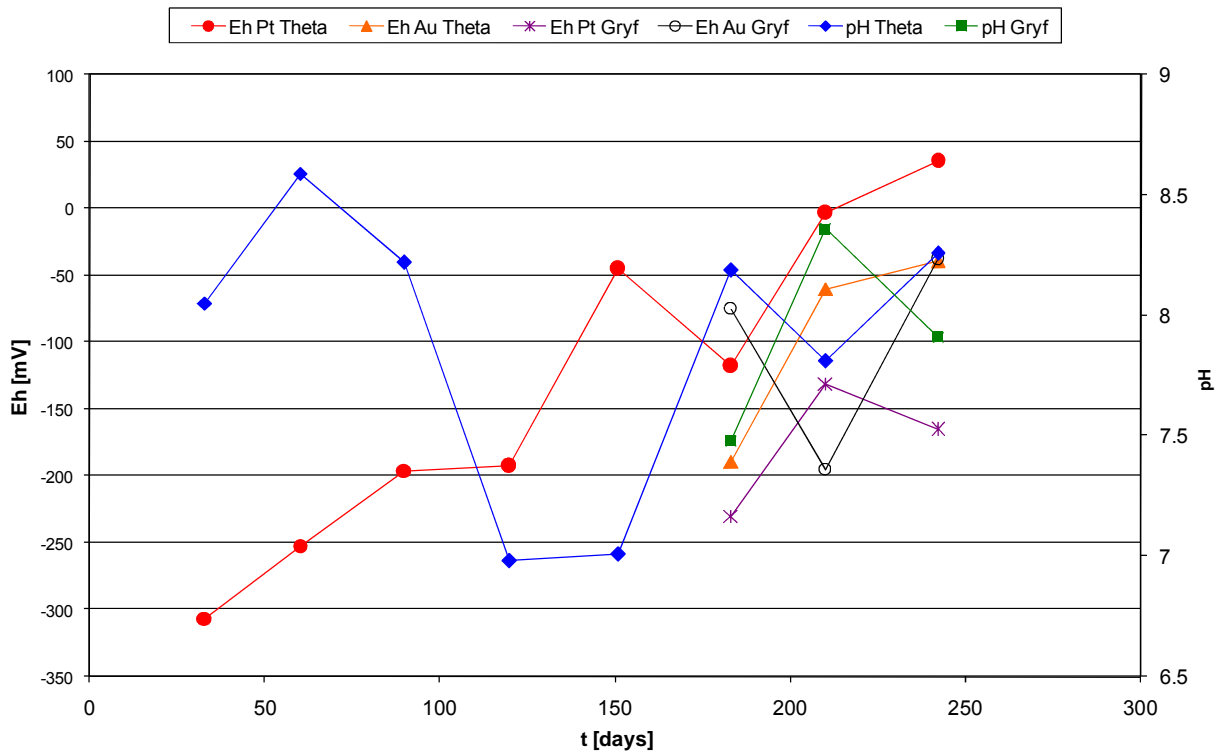


Fig. 4: Results of measuring Eh and pH of the solution

After finishing the experiment, the average corrosion rate will be determined from the weight loss of the sample.

These preliminary results show that the rate of hydrogen evolution changes significantly over time. The very high hydrogen evolution rate at the very beginning could be connected with the fast formation of protective corrosion product layer on the surface of carbon steel sample. The hydrogen evolution rate during the 50 days is little higher in a comparison with our previous results with carbon steel (see deliverable D.2.3). The reason will be sought after finishing the experiment. The hydrogen generation rate further decreases slightly below $1 \text{ mol m}^{-2} \text{ yr}^{-1}$ after 50 days, probably with the formation of a thicker corrosion product layer. But even this value is by order of magnitude greater than the value obtained before in our laboratory, when the experiments were not conducted in the aerobic box or in other laboratories (Hunter et al, 2007). Nevertheless, the results of hydrogen generation were several times checked out in respect of possible experimental mistake in measuring of volume changes, but no error was found. Furthermore, there was not find any evidence for galvanic corrosion after the experiments dismantling. The results obtained will be more carefully analyzed on the basis of additional characterization after dismantling and determination of the corrosion rate by weight loss measurements.

1.3 HYDROGEN MIGRATION THROUGH COMPACTED BENTONITE

1.3.1 Introduction

Despite a large number of publications (see D1.2) devoted to the study of migration of hydrogen through compacted bentonite, the experimental evidence is still not sufficient to fully understand the mechanism of hydrogen flow through compacted bentonite, predict, with some certainty, maximal possible pressure achieved by gas accumulation between canister and bentonite or to determine the character of preferential paths created by gas transport. This was also the reason, why NRI decided to utilise the equipment developed first for measuring hydrogen generation rates to measuring hydrogen migration through compacted bentonite. In the first experiments compacted bentonite was simply put to close the outlet from hydrogen generation so that hydrogen had to pass through compacted bentonite. These experiments were lately also completed with experiments with backpressure and with constant pressure of hydrogen from a hydrogen reservoir.

1.3.2 Experimental method

Devices developed in NRI for measuring hydrogen migration through compacted bentonite are shown in Fig. 5 and 7. For the first two devices, hydrogen generated by reaction of iron powder (Alfa Aesar A Johnson Matthey Company (< 10 micron, 99.9+% (metal basis), surface 0.205 m^2/g) with water was forced to pass through compacted, saturated bentonite. Various types of bentonite (Czech Ca, Mg bentonite from deposit Rokle, or Na bentonite, Volclay KWK 20-80, MX-80) were saturated under pressure for several days. The density of bentonite samples was in the range from 1200 to 1750 kg/m^3 . But most of the experiments were conducted with Czech bentonite Rokle compacted to density of 1600 kg/m^3 .

The composition of bentonites used in experiments are given in the following Table 3.

Table 3: Mineralogical composition of tested bentonites

Oxide	Rokle raw	Rokle Sabenil 75	Volclay KWK 20-80	Volclay from Voltex system
SiO ₂	48.06	51.91	61.75	56.52
Al ₂ O ₃	14.73	15.52	20.5	18.75
TiO ₂	3.98	2.28	0.22	0.3
Fe ₂ O ₃	11.97	8.89	3.87	4.19
FeO	1.50	2.95	1.02	2.66
MnO	0.13	0.108	0.01	0.03
MgO	2.21	2.22	2.58	1.59
CaO	4.88	4.6	0.94	4.75
Na ₂ O	0.30	1.21	2.08	2.1
K ₂ O	1.09	1.27	0.59	0.79
P ₂ O ₅	0.80	0.4	0.22	0.16
S	0.03	0.09	-	0.39
CO ₂	1.12	5.15	0.33	3.3

The hydraulic conductivities acquired during sample saturation are given in Table 4.

Table 4: Hydraulic conductivities of bentonites

Bentonite	Dry density [kg.m ⁻³]	Saturation pressure [MPa]	Coefficient of permeability [m.s ⁻¹]
Rokle raw	1600	15	1.4E-13
Rokle Sabenil B-75	1600	15	1.8E-13
Volclay KWK 20-80	1600	15	3.0E-14
Volclay from Voltex system	1600	15	7.9E-14
MX 80	1600	15	4.2E-14

In the first device (Fig. 5), change of volume caused by hydrogen evolution and its passing through compacted bentonite was measured by LVTD Displacement Transducer. The pressure source for holding a constant pressure is a heavy piston, moving in mutually interconnected pressurized cylindrical vessels with a rolling membrane (Brůha and Pelech, 1989). The volume measurement is based on detecting the piston position, which depends on the medium volume.

In the second device (Fig. 6), the change of volume due to hydrogen evolution and passing through bentonite was detected by displacement of piston of digital compression testing machine, which held a constant backpressure.

In the third device (Fig. 7) source of constant pressure of hydrogen was from hydrogen reservoir and kept using Husk pump.

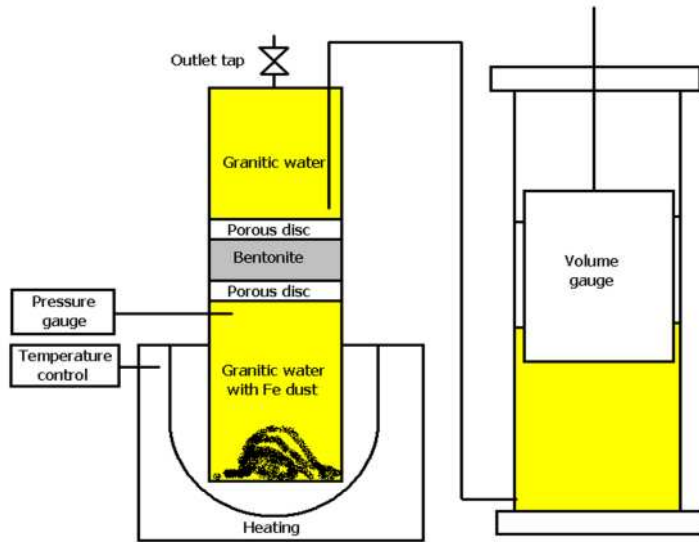


Fig. 5: Scheme of device for measuring hydrogen migration without backpressure

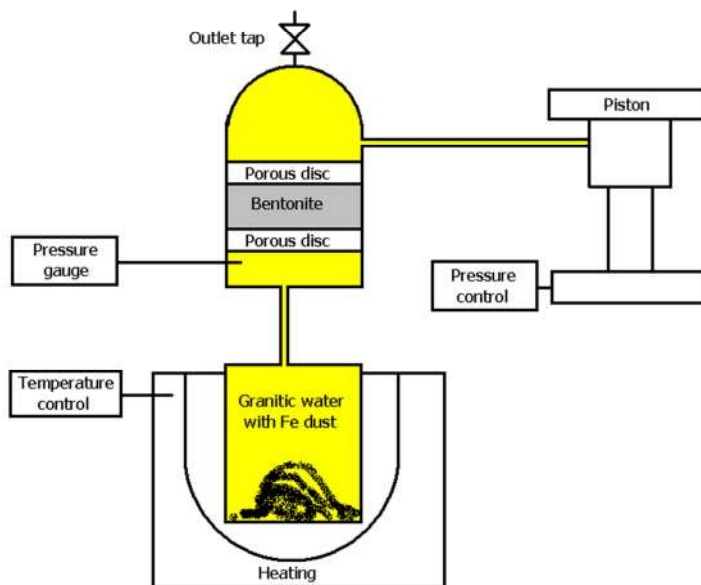


Fig. 6: Scheme of device for measuring hydrogen migration with backpressure from compression machine

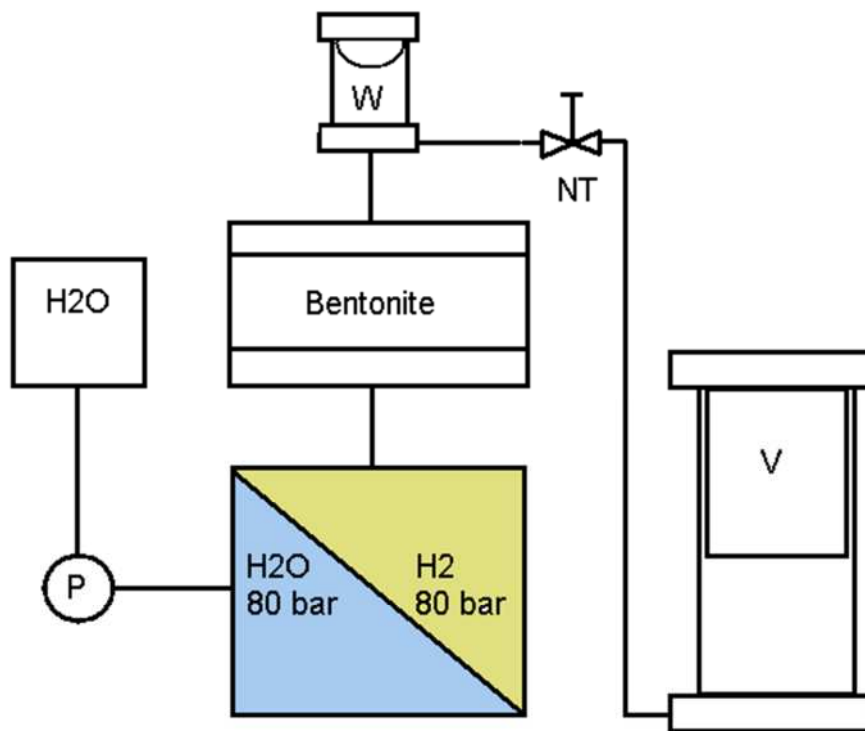


Fig. 7: Device for measuring hydrogen migration from a hydrogen reservoir under constant pressure (P – pump, W – plexi window, NT – needle valve, V – volume gauge)

1.3.3 Results and Discussion

The results of the experiments with bentonite from deposit Rokle of various densities in the range from 1200 to 1750 kg/m³ conducted using device shown in Fig. 5 are shown in Fig. 8. In this device hydrogen passes through saturated, compacted bentonite from the pressure created by hydrogen from iron corrosion in corrosion vessel below bentonite to constant near atmospheric pressure above bentonite. The higher density of bentonite, the higher pressure needed for the hydrogen to break through bentonite. For all densities of bentonite several breakthrough cycles can be observed before hydrogen is passing through bentonite without any further breakthrough cycles or all iron was consumed. It can be also seen that for bentonite of high density (1600 and 1750 kg/m³) some pressure plateau before the first breakthrough was formed. It indicates an increase of volume caused by the deformation and/or desaturation of bentonite before hydrogen breakthrough. The pressure for further breakthrough decreases with the number of breakthroughs.

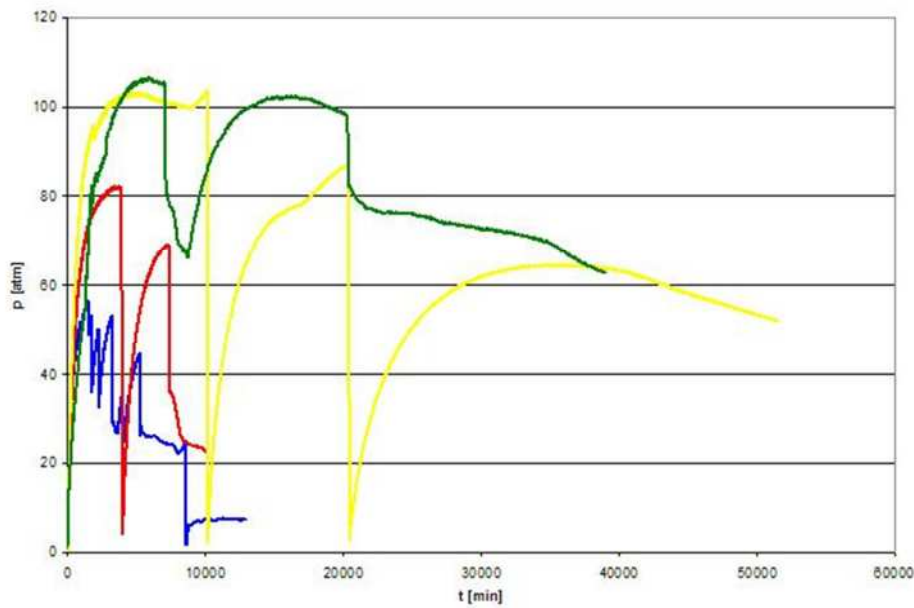


Fig. 8: Hydrogen breakthrough pressure curves for samples of bentonite Rokle of various densities

Some experiments were repeated under the same conditions, but it was difficult to obtain precisely the same results. In Fig. 9 breakthrough curve for bentonite Rokle with density of 1600 kg/m³ is shown. It can be seen that the character of curve is the same as the bentonite of the same density shown in Fig. 8, but the values of critical pressures and number of breakthroughs are different. It supports the hypothesis that the character of gas penetration depends on heterogeneity of bentonite and the nature of initial defects in bentonite samples (Delahay and Alonso, 2002). The critical pressure of the breakthrough is much larger than initial swelling pressure (45 bar) determined for Rokle bentonite of density 1600 kg/m³.

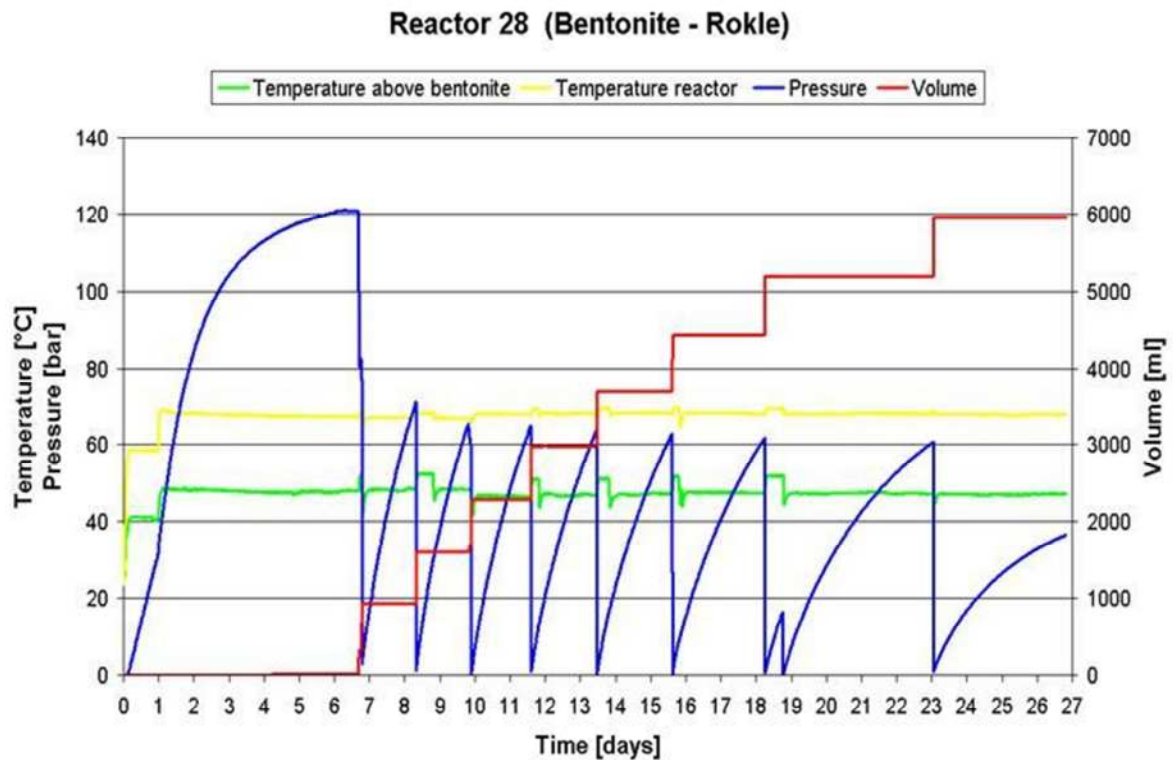


Fig. 9: Breakthrough curve for bentonite Rokle of density 1600 kg/m³

The breakthrough curves for Na-bentonite (Volclay KWK 20-80) compacted to density of 1600 kg/m³ and MX -80 bentonite compacted to the same densities are shown in Fig. 10 and 11.

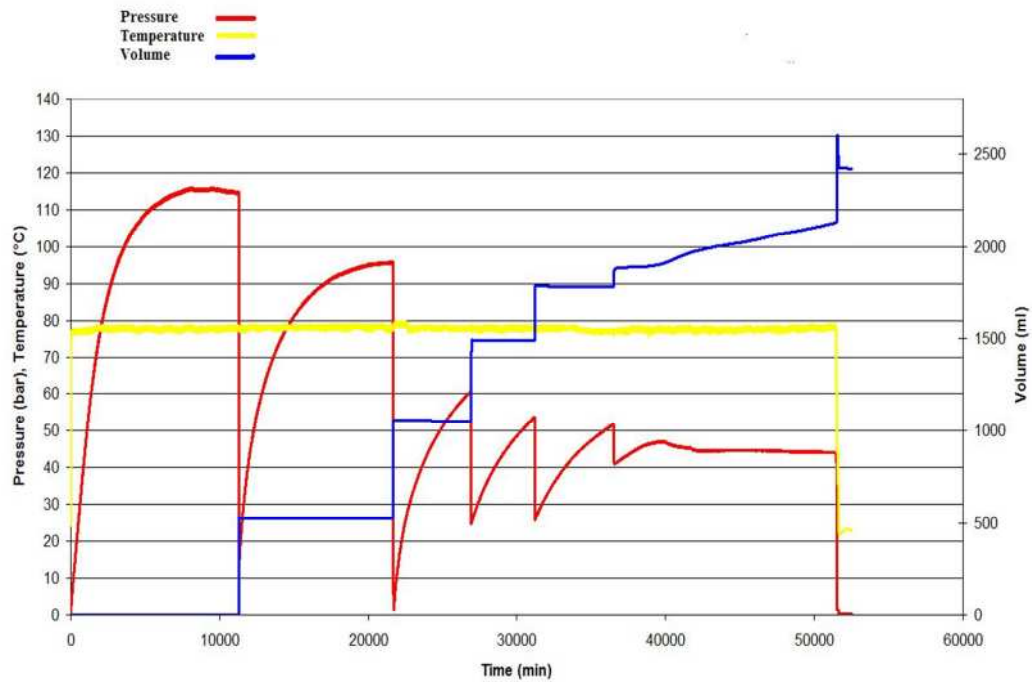


Fig. 10: Breakthrough curve for Wyoming type bentonite (Volclay KWK-20-80) with dry density 1600 g/cm³

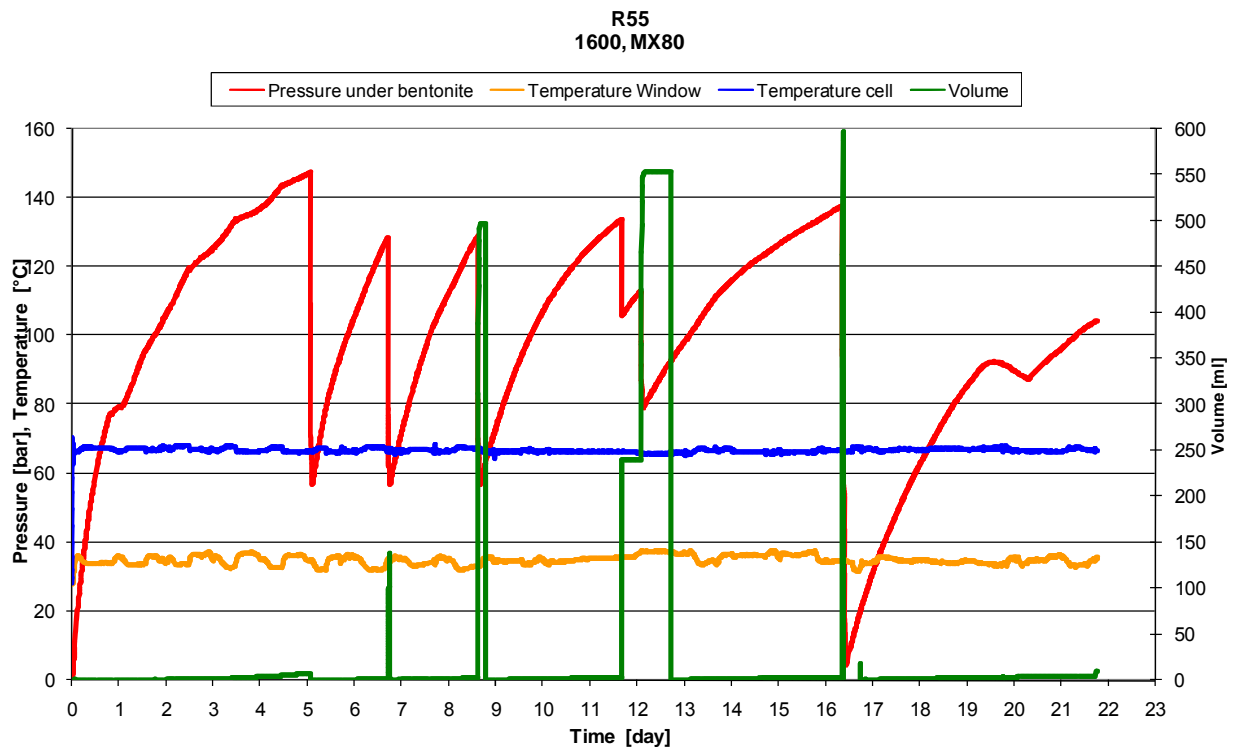


Fig. 11: Breakthrough curve for MX-80 bentonite (1600 kg/m³)

It can be seen that during breakthroughs lasting several minutes hundreds of ml of hydrogen can pass through compacted bentonite (green curves).

Details of penetration of hydrogen through compacted bentonites Volclay KWK-20-80 and Rokle are given in Fig. 12 and 13. Breakthroughs itself were very fast. During less than two minutes almost 500 ml of hydrogen passed through bentonites. Immediately after breakthrough it was easily seen that water was very quickly sucked back to bentonite. This suggests that breakthrough is connected with desaturation of bentonite. It can be also seen that before breakthrough the flux of hydrogen through saturated Na-bentonite, Volclay KWK-20-80 is smaller than flux of hydrogen through Ca,Mg- bentonite, Rokle of the same density.

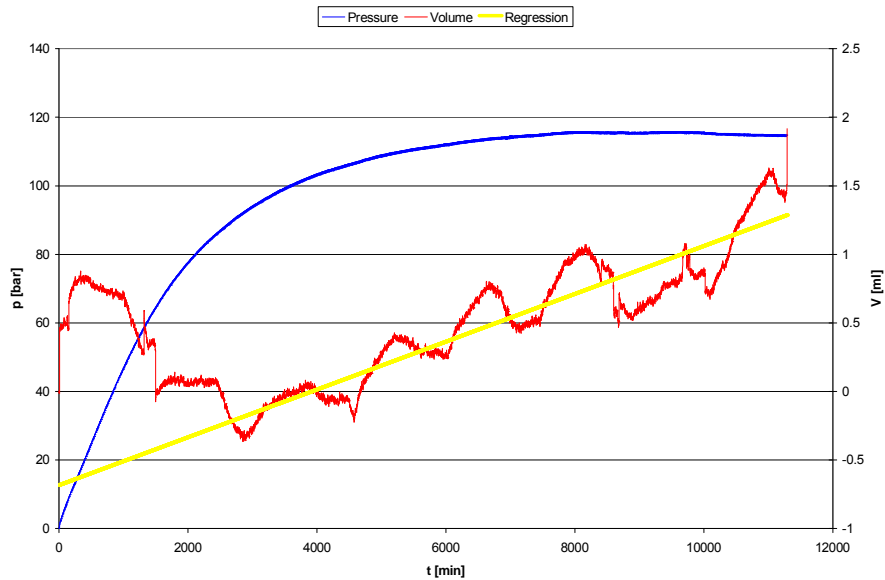


Fig. 12: Change of pressure and volume due to release of hydrogen for Wyoming type (Volclay KWK-20-80) bentonite before the first breakthrough

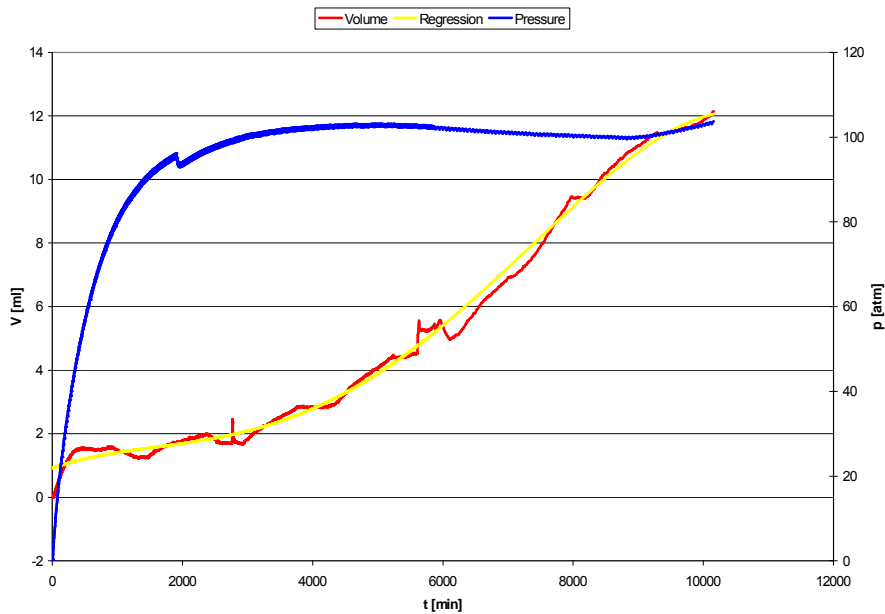


Fig. 13: Change of pressure and volume due to release of hydrogen for Rokle type bentonite before the first breakthrough

From the change of volume of hydrogen passed through bentonite permeability can be calculated according to the following equation (Horseman et al., 1999):

$$Q_{st} = \frac{v_{mst} k_g A_s}{2\mu_g L_s RT} \left[p_{gi}^2 - (p_{wo} + p_{co})^2 \right] \quad (1)$$

where Q_{st} ($m^3 \cdot s^{-1}$) is the volumetric flux of gas at standard temperature and pressure (STP), v_{mst} ($m^3 \cdot mol^{-1}$) is the molar volume of the gas at STP, μ_g ($Pa \cdot s$) is the dynamic viscosity of the gas, R ($J \cdot mol^{-1} \cdot K^{-1}$) is the gas constant, T (K) is the absolute temperature, p_{gi} (Pa) is the upstream gas pressure, p_{wo} (Pa) is the downstream water pressure, p_{co} is the apparent value of matric suction and A_s (m^2) and L_s (m) are the cross-sectional area and length respectively of the test specimen. For simplification p_{wo} was considered to be slightly higher than atmospheric pressure (1.15×10^5 Pa) and p_{co} was not considered in calculations because after breakthrough the pressure goes practically to zero values. The permeabilities values obtained were 2.6×10^{-19} and $7.1 \times 10^{-18} m^2$ for Volclay and Rokle bentonite, respectively.

The flux of hydrogen through bentonite before breakthrough can be, however, described also by diffusion according to the following equation:

$$J = -D(dc/dx) \quad (2)$$

where J is the flux density of hydrogen ($mol \cdot m^{-2} \cdot s^{-1}$), D is Fickian mass transport coefficient ($m^2 \cdot s^{-1}$), c is chemical concentration of hydrogen in aqueous phase ($mol \cdot m^{-3}$) and x is the distance over which a concentration gradient is being considered (m). We can suppose that before breakthrough, the concentration of hydrogen entering bentonite corresponds to the pressure of hydrogen according to Henry law. With the assumption of almost zero concentration of hydrogen at atmospheric pressure, diffusion coefficients $2.9 \times 10^{-11} m^2 \cdot s^{-1}$ and $3.7 \times 10^{-10} m^2 \cdot s^{-1}$ for Volclay KWK-20-80 and Rokle bentonite, respectively can be obtained.

It is difficult to differentiate between advection and diffusion in this case, because driving forces for flow are in principle the same for both processes, i.e. hydrogen accumulation before bentonite.

The results of pressure increase of waterproofing system (red line) and volume change (green line) of commercial Na-bentonite, designed Volclay from Voltex waterproofing system are shown in Fig.14. Breakthrough was not reached in the experiment lasting 19 days. The pressure stabilized around 18 MPa. The experiment was stopped because water consumption in reaction with iron powder. This was confirmed after dismantling the cell by finding that iron and iron corrosion products in the cell were dry. The results obtained are different from the results obtained with Volclay KWK-20-80.

R51

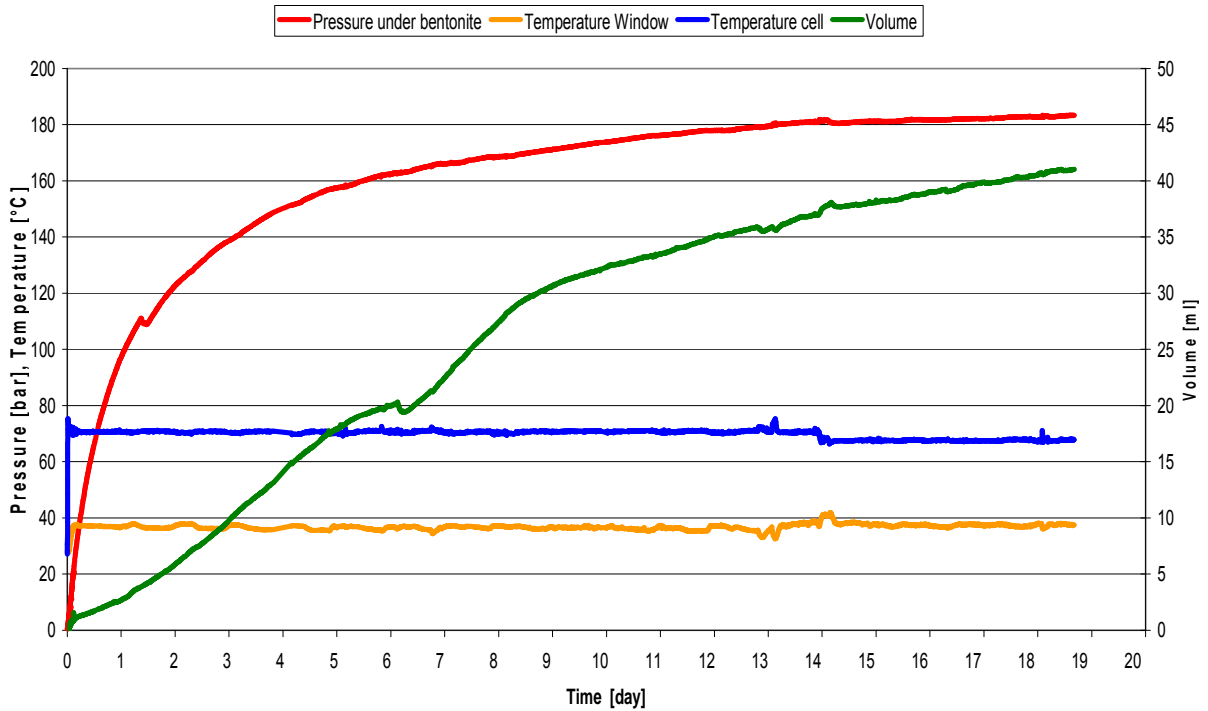


Fig. 14: Pressure and volume increase of Volclay bentonite from Voltex waterproofing system due hydrogen generation

Small flux of hydrogen through compacted bentonite can be observed before breakthrough. It correspond to permeability $2.2 \times 10^{-24} \text{ m}^2$ (Eq. 1) or diffusion coefficient $8 \times 10^{-11} \text{ m}^2 \text{ s}^{-1}$ calculated according to the equation (2). (Fig. 9). These values are not very much different from the values of Volclay KWK-20-80 ($6.1 \times 10^{-24} \text{ m}^2$ and $2.9 \times 10^{-11} \text{ m}^2 \text{ s}^{-1}$). The pressure could possible rise further if the water had not been consumed.

The results of the experiment carried out with commercially treated bentonite Rokle B75 is shown in Fig. 15. The breakthrough was observed much earlier than in the case of raw Rokle samples studied before and at much lower pressure (see Figs. 7 and 8), but the pressure after the first breakthrough does not drop to zero so that probably only a very small fracture was created due to a possible initial defect in the sample. Before the breakthrough only very low amount of hydrogen passed through the sample (2 ml/day). After the breakthrough a stable value of pressure below bentonite and almost linear flux of hydrogen was settled (350 ml/day) (Fig. 16). The permeability calculated according to equation (1) with the assumption of a constant pressure difference 8.8 MPa approximately $3.5 \times 10^{-21} \text{ m}^2$ was calculated, i.e. the value of two-order of magnitude higher than before breakthrough.

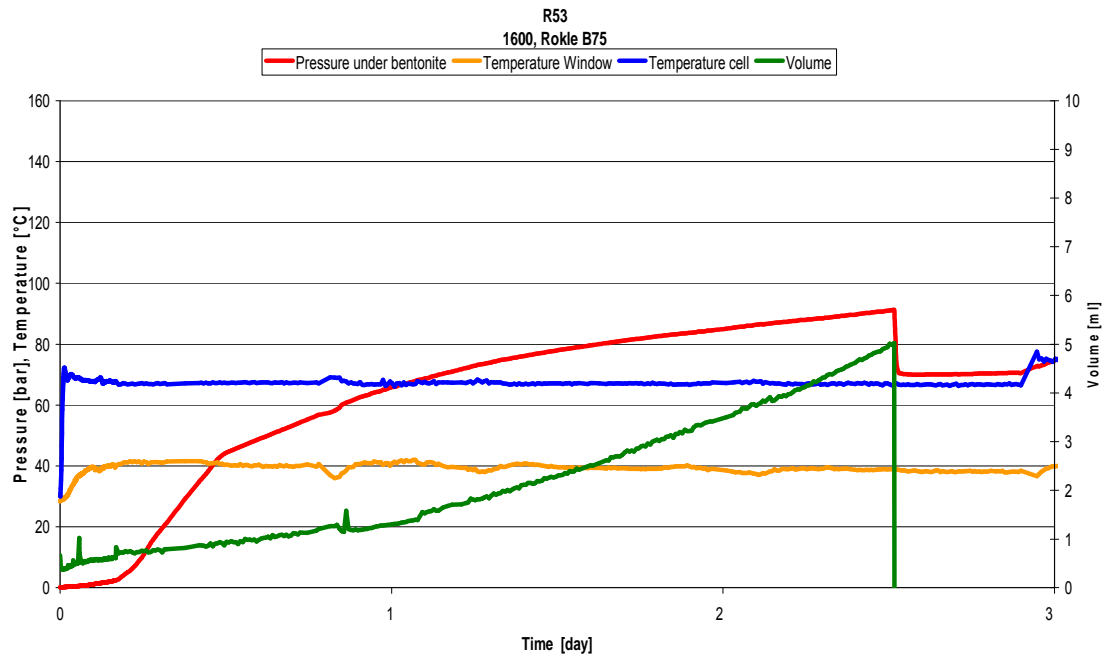


Fig. 15: Pressure and volume change due to hydrogen transport in bentonite Rokle 75 (before the first breakthrough)

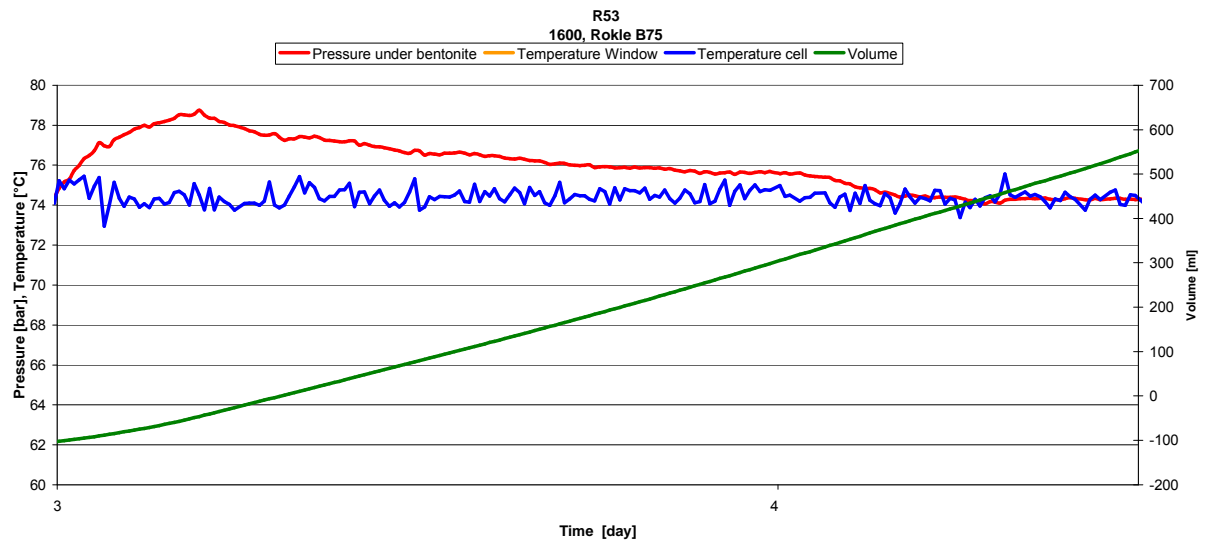


Fig. 16: Pressure and volume change after the first breakthrough in Rokle 75

The experiment had to be stopped due to the consumption of water when no hydrogen was generated.

All the experiments with source of hydrogen from iron powder corrosion are possibly affected by an uncertain rate of hydrogen generation, affected by the amount of initial oxygen dissolved in water, iron surface change or water availability. Therefore a device (Fig.7) enabling to conduct experiments under constant pressure of hydrogen was developed. The samples of Rokle B 75 of density 1600 kg/m^3 had diameters 30 mm and 100 mm, respectively.

A comparison of hydrogen flux of samples of diameter 3 and 10 cm is shown in Fig. 14. It can be seen that the applied pressure changes very little in experiments (see red and blue lines in Fig. 17).

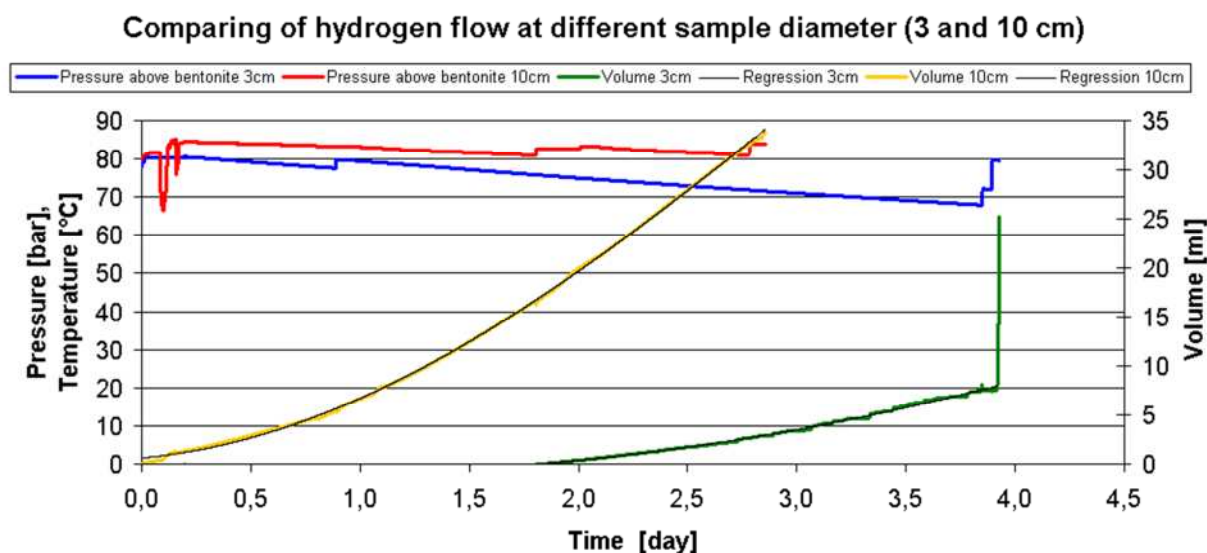


Fig. 17: Hydrogen flow through compacted, saturated bentonite (Rokle) at hydrogen pressure of 8 MPa

It can be seen that the beginning and the rate of measurable flux of hydrogen through bentonite depends slightly on dimension of samples. The measurable hydrogen flux for a larger sample (10 cm of diameter) started immediately after the pressure of 8 MPa was applied, the rate of hydrogen flux increased until breakthrough after 3 days. The average flux of hydrogen $2.5 \times 10^{-8} \text{ m}^3/\text{m}^2\text{s}$ derived from approximately linear part of the curve corresponds to permeability of $1.4 \times 10^{-23} \text{ m}^2$, but it can be also described by diffusion with diffusion coefficient $3.4 \times 10^{-10} \text{ m}^2\text{s}^{-1}$. In the case of the smaller sample (green line) the measurable hydrogen flux started later, approximately after 2 days. The flux of hydrogen $9 \times 10^{-8} \text{ m}^3/\text{m}^2\text{s}$ corresponds to permeability $4.9 \times 10^{-23} \text{ m}^2$ or diffusion coefficient $9 \times 10^{-10} \text{ m}^2\text{s}^{-1}$.

1.4 CONCLUSIONS

The preliminary results of the long-term experiment with hydrogen generation showed that hydrogen generation under anaerobic conditions decreases over time, but the values are approximately one order of magnitude higher ($1 \text{ mol m}^{-2} \text{ yr}^{-1}$ corresponding to $5.55 \text{ } \mu\text{m}/\text{y}$) than expected in some of recent reports (e.g. Hunter et al, 2007). This will have to be confirmed by weight loss measuring after dismantling the equipment and comprehensive analyses of all the results obtained.

The results of our hydrogen migration study suggest that:

- 1) The first transport of hydrogen through compacted bentonite before breakthrough by diffusion in aqueous phase depends on the type and density of bentonite. Diffusion coefficients of Ca, Mg bentonite (Rokle bentonites) of density $1600 \text{ kg}/\text{m}^3$ are around $5 \times 10^{-10} \text{ m}^2\text{s}^{-1}$, one order of magnitude lower are diffusion coefficients for Na- bentonites (Volclay type) ($3 \times 10^{-11} \text{ m}^2\text{s}^{-1}$). But it is not easy to tell whether it is diffusion or advection, because driving forces for flux are the same: the amount of hydrogen accumulated before saturated bentonite.
- 2) The second phase of hydrogen transport in the gas phase during breakthrough also depends on density and type of bentonite. Generally speaking, the lower density, the

earlier breakdown and lower maximal pressure achieved, but is difficult to predict. It was impossible to get the same results with the same type bentonite. This probably connected with heterogeneity of bentonite and possible initial defects. Permeabilities during breakthroughs were in the range from $2 \times 10^{-22} \text{ m}^2$ to $7 \times 10^{-18} \text{ m}^2$.

- 3) In the experiments with constant pressure of hydrogen earlier breakthrough was observed in a larger sample. The reason could be also connected with greater number of initial defects in larger samples. This suggests an importance of the scale effect.

2 IRSN Experiments

The objective of the irradiation experiments carried out by IRSN within FORGE is to examine the influence of gamma radiation on hydrogen generation by corrosion of carbon steel. Previous period was devoted to develop and test an appropriate experimental setup, a major constraint being on-line measurements of hydrogen together with irradiation conditions. This report presents hydrogen production rates obtained in two experiments conducted at two dose rates, respectively 50 and 100 Gy/h, chosen in order to enhance phenomena.

2.1 EXPERIMENTAL METHOD

After different tests (see deliverable D2.3), a new experimental cell (stainless steel) was developed which allows degassing of solubilised gases, control of both pressure and temperature in the cell, as well as continuous measurement of gas produced in the cell.

A scheme of the whole experimental setup, developed in 2010-2011, is presented in Fig. 18.

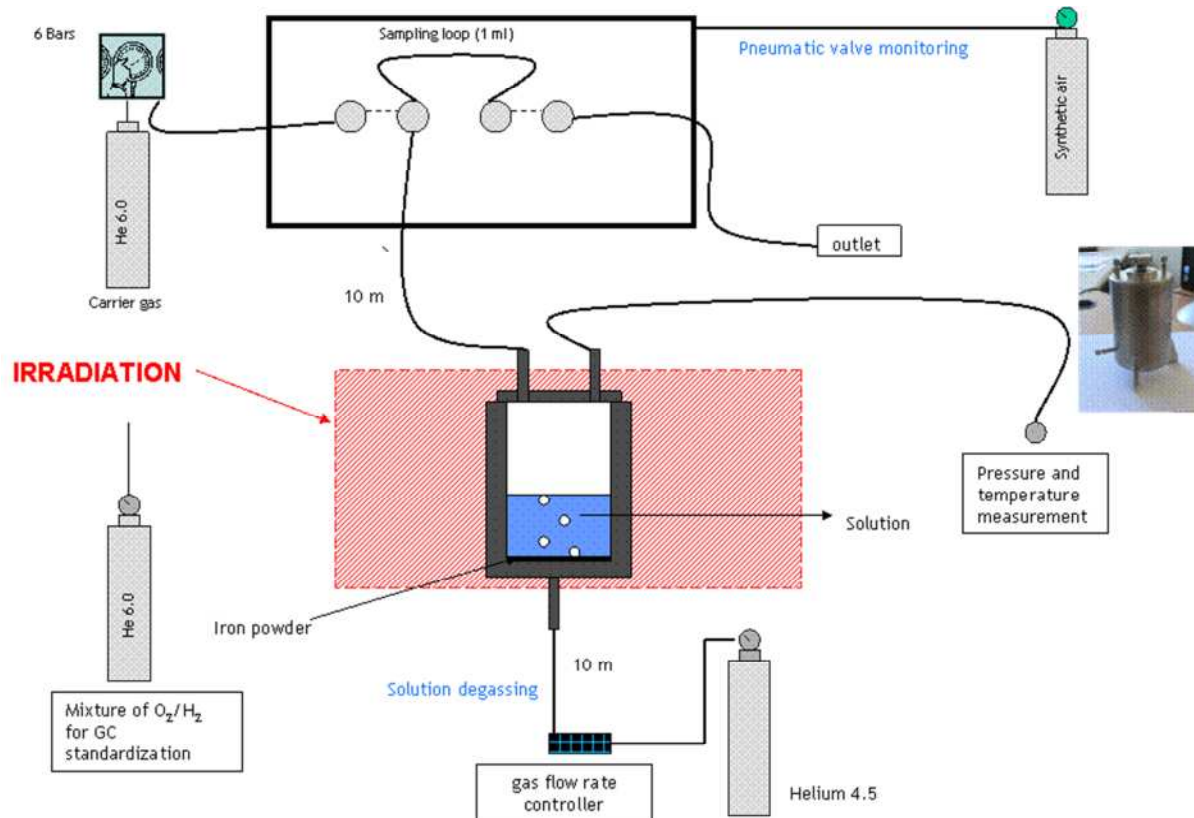


Fig. 18: Experimental device

A mass close to 10 g of iron powder (particle diameter < 210 μm) provided by Alfa Aesar is added to a given volume (100 ml) of de-aerated water (Milli-Q quality). The degassing of the solution is ensured by Helium 4.5 at a constant flow rate (5ml/min). The gas mixture (H_2 , O_2 , N_2 in helium) was regularly (10 min) sampled (1 ml) and analysed by Gas Chromatography (Varian GC 450). The column was filled with molecular sieve and the detector is a Pulsed Discharge Helium Ionised Detector (PDHID). Helium 6.0 was used as carrier gas. Gas chromatography was calibrated with a mixture of gas ($[\text{H}_2] = [\text{O}_2] = 50 \text{ ppm}$ in He 6.0). The detection limit for each gas was 0.1 ppm in He 6.0.

The experiment progress is plotted in Fig. 19. Step 1 corresponds to a pure corrosion phase. This step is achieved as soon as the hydrogen production is constant. Then irradiation is applied (Step 2) for at least 3 weeks. The optimal duration corresponds to the time necessary to obtain a plateau (like in Step 1). When irradiation is stopped, ideally hydrogen release is measured until to obtain also a plateau (Step 3). Each experiment needs at least 6 weeks. However, it was necessary to stop irradiation before to reach a plateau because of the availability of IRMA (irradiation facility).

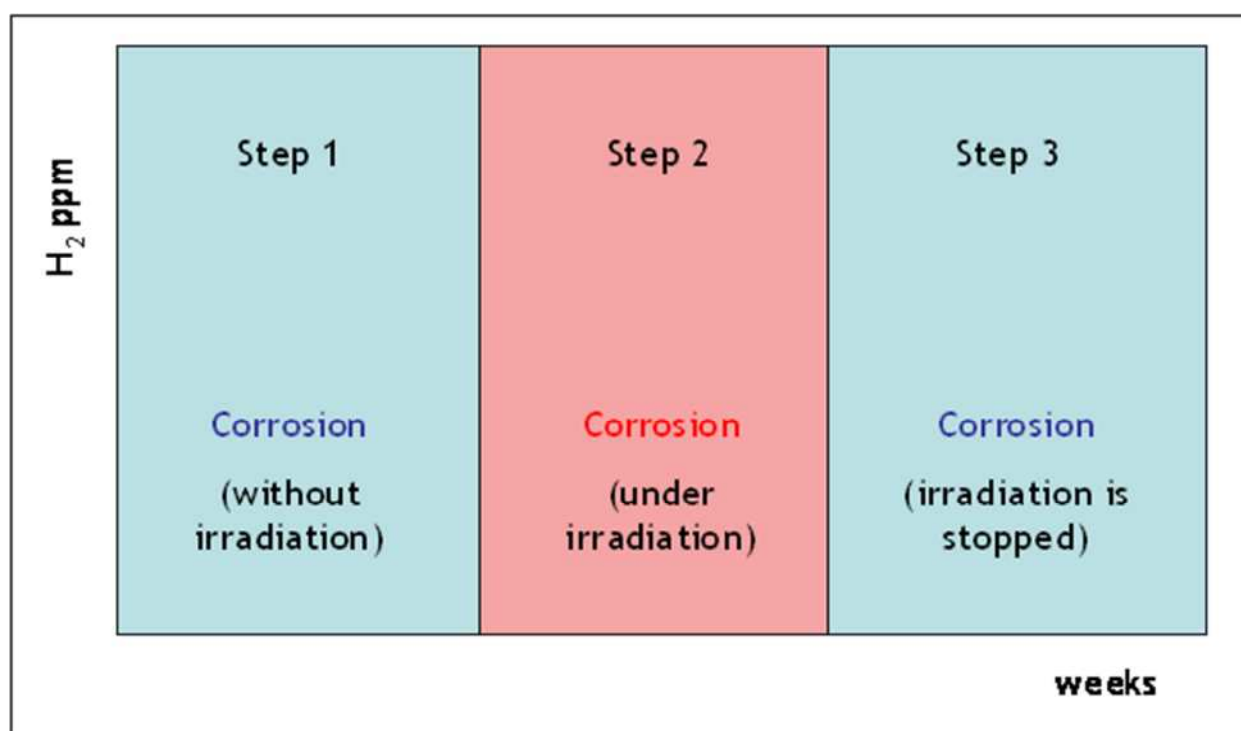


Fig. 19: Steps of an experiment

At the end of the experiment, the cell is dismantled and both solution (pH, redox potential, conductivity) and solid (Raman spectroscopy) are analysed.

The quantification of H_2O_2 according to Ghormley method (Joseph et al. 2008) was not useful for solutions containing soluble iron species, and H_2O_2 concentration was estimated for one experiment with specific indicators (Merck). Because of their poor sensibility, the development of a new method appeared necessary.

2.2 RESULTS

Two dose rates (respectively 100 and 50 Gy/h) were applied to the same mixture of pure de-aerated water/ Fe(0) powder. The results expressed as hydrogen concentration in helium (in ppm) versus time (in min) are plotted on Fig. 20 - 21.

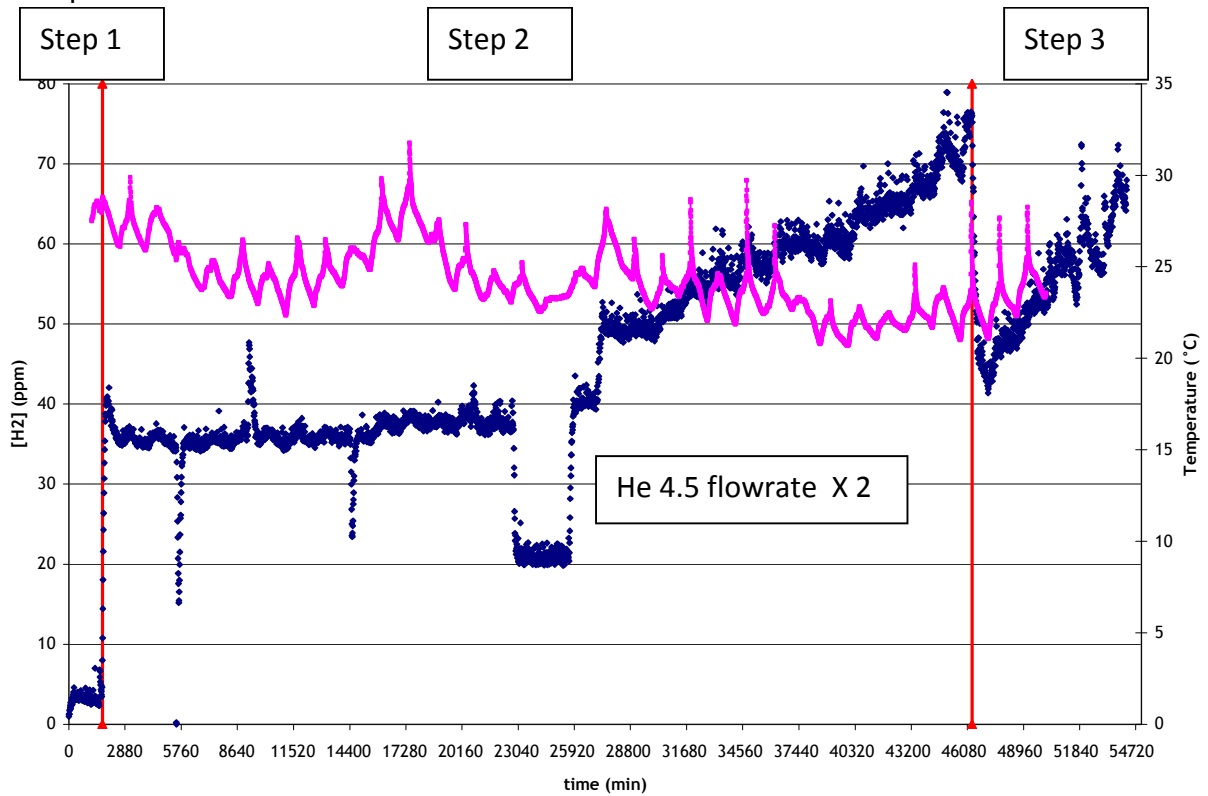


Fig. 20: Hydrogen release versus time $M_{Fe} = 10 \text{ g}$, $V_{H_2O} = 100 \text{ ml}$ – dose rate = 100 Gy/h

For the two curves, the same shape is observed. A first plateau is obtained after 1 day (corresponding to a pseudo-steady state corrosion rate). As soon as irradiation begins, H_2 production increases sharply due to water radiolysis, until to reach a new plateau corresponding to the sum of hydrogen produced by corrosion with that produced by water radiolysis. For the higher dose rate, the plateau lasts 16 days while for the lower dose rate, the plateau is only 2 days long. Then an increase of hydrogen release is observed for the two dose rates, globally continuous except for the low dose rate experiment which also includes a pseudo plateau lasting 5 days before irradiation was stopped.

When irradiation is stopped, H_2 production rate decreases (same amplitude of decrease than the amplitude of increase observed at the beginning of irradiation due to water radiolysis), and then increases again without to reach a plateau (1 week for 100 Gy/h experiment and 2 weeks for 50 Gy/h experiment).

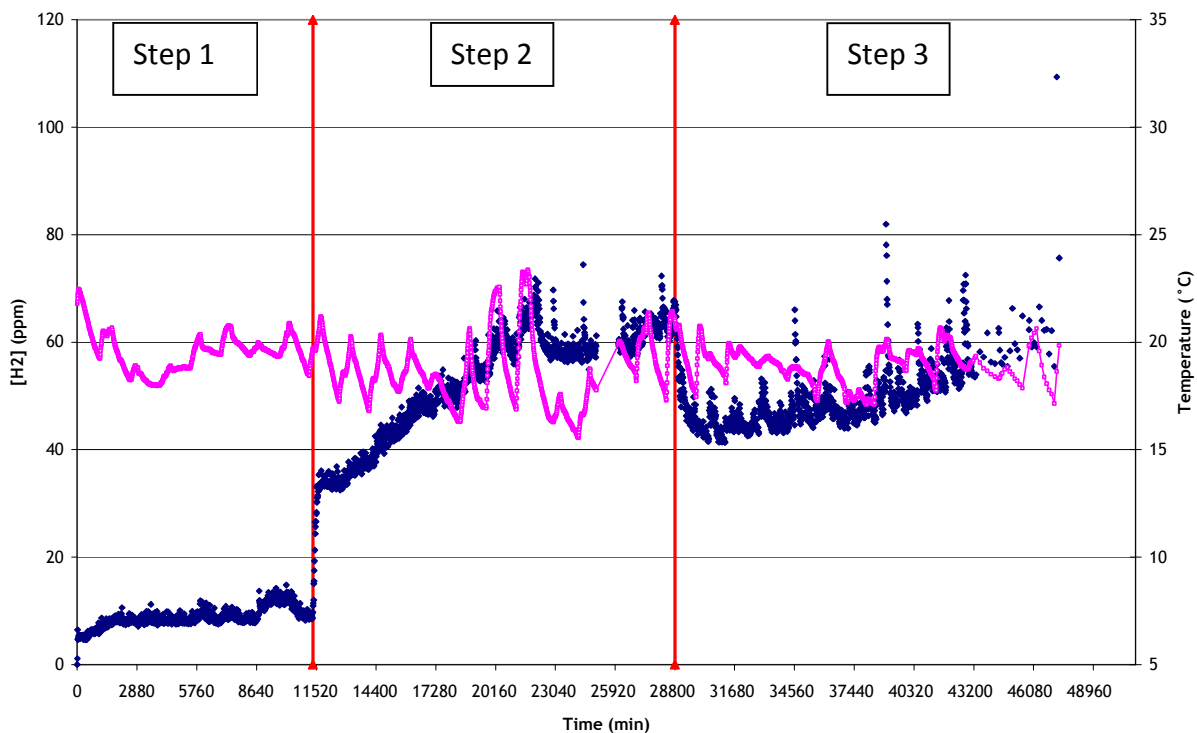


Fig. 21: Hydrogen release versus time $M_{Fe} = 10\text{ g}$, $V_{H_2O} = 100\text{ ml}$ – dose rate = 50 Gy/h

The solutions at the end of these experiments were analysed (Table 5). For both experiments, the solutions were alkaline ($\text{pH} > 11$). The conductivity value was linked to the release of Fe II/III in solution. The redox potential values are slightly oxidizing but considering the conditions of measurement (contact of solution with atmosphere), we can assume that the redox potential in the cell was reducing.

Table 5: Solution analysis

Experiment	Total dose	pH	Eh (mV)	Conductivity g/l	H ₂ O ₂ (mg/l)
50 Gy/h	14.6 kGy	10.98	13.3	1.19	NM
100 Gy/h	74.4 Gy	11	80	NM	0.5

NM: Non Measured

Raman spectroscopy on one solid (experiment 100Gy/h) didn't show any iron phase (oxy-hydroxide), probably because the modifications are limited (only 2 months) and cannot be detected (below the resolution of this technique).

2.3 DISCUSSION

In order to compare H₂ production for the two experiments, we have plotted H₂ release (mol/min) versus time (min) in Fig.22.

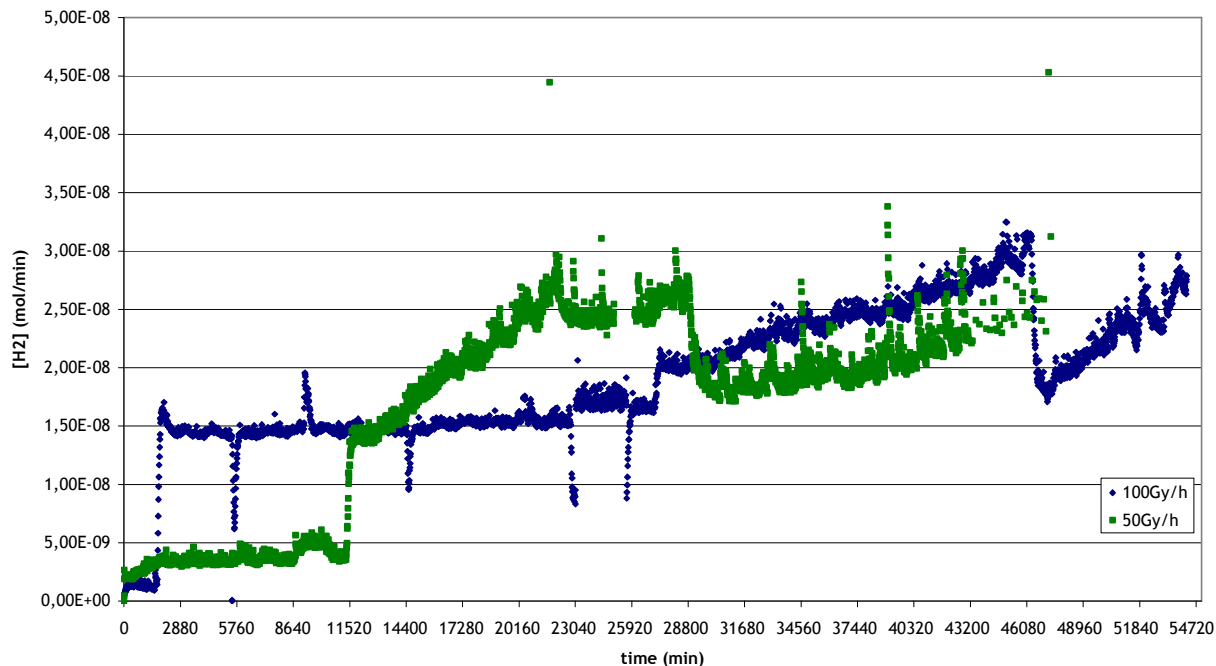
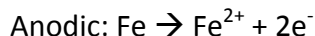
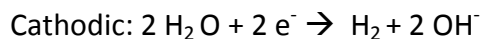


Fig. 22: Hydrogen production rate (mol/min) versus time (min)

Step 1 - Corrosion without irradiation

Experiments were conducted in pure de-aerated water (deaerated by boiling)). Therefore anaerobic corrosion takes place according to the following reactions:



A corrosion layer is expected to form at the surface of the iron particles, mainly constituted of magnetite Fe_3O_4 .

Corrosion rates deduced from these experiments are gathered in Table 6.

Table 6: H₂ production rate during step 1 for the two experiments

Dose rate (Gy/h)	H ₂ (mol/min)	Corrosion rate (mol/g.y)	Corrosion* rate (mol/m ² .y)	Corrosion rate (µm/y) deduced from (1)
50	$3.81 \cdot 10^{-9}$	$2.0 \cdot 10^{-4}$	$5.57 \cdot 10^{-2}$	0.4
100	$1.37 \cdot 10^{-9}$	$7.2 \cdot 10^{-5}$	$2 \cdot 10^{-2}$	0.14

*Specific area was estimated to 0.0036 m²/g.

Iron corrosion rates for the two experiments are slightly different (factor ~ 3). However, in the “100 Gy/h” experiment, the corrosion rate was estimated through only 1 day hydrogen measurement and is probably underestimated.

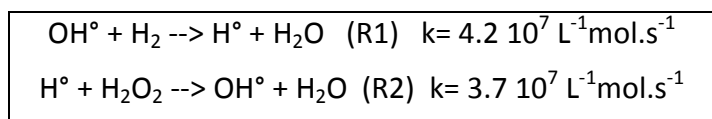
The corrosion rates (expressed in $\mu\text{m/y}$) are lower than those determined by NRI (see deliverable D2.2) but are globally consistent with values reported in literature (see deliverable D2.1)

Step 2 - Irradiation step: water radiolysis

Water radiolysis produces free radicals such as e_{aq}^- , H^\bullet , OH^\bullet , H^+ , HO_2^\bullet and molecular products such as H_2 and H_2O_2 . The steady-state concentration of radiolysis products depends on their radiolysis production rate and recombination reactions (Yakabuskie et al. 2010).

In a completely closed single-phase situation almost never encountered in practice, the irradiation of pure water produces no overall oxidizing and reducing effect and low steady state concentrations are obtained according to Allen chain (Table 7).

Table 7: Allen chain



Our experiments were conducted in “open conditions”, i.e. produced gas was continuously removed from the solution. Therefore, recombination reactions are limited and Allen chain is disturbed.

In our experiments, when irradiation begins, water radiolysis occurs and the production of hydrogen increases sharply until to reach a plateau. If we subtract the contribution of corrosion to the values obtained on the plateau, H_2 production by water radiolysis can be estimated (Table 8).

H_2 being a primary product of radiolysis, its production rate is directly proportional to the dose rate and can be calculated according to the equation:

$$d[H_2]/dt = C_{ste} \cdot D \cdot G_{H_2} \cdot V$$

$$d[H_2]/dt \text{ in mol/min}$$

$$C_{ste} = \text{conversion term} = 6.22 \cdot 10^{-6}$$

$$D = \text{Dose rate (Gy/s)}$$

$$G_{H_2} \text{ is the radiolytic yield} = 0.45 \text{ molecules/100eV for } \gamma \text{ irradiation (Joseph et al. 2008)}$$

$$V = \text{volume of solution (L)} = 0.1$$

The values deduced from experiments are higher than those calculated (Table 8). Moreover, H_2 produced by radiolysis being proportional to the dose rate, a factor 2 between the 2 experiments is expected instead of 1.4.

In slightly aerated conditions H_2 production by water radiolysis is higher than in de-aerated ones (disturbance of Allen chain). It is possible that in one experiment (50 Gy/h), oxygen still remains in solution inducing higher amount of H_2 production.

Table 8: Hydrogen production by water radiolysis in mol/min

Dose rate (Gy/h)	Measured H ₂	Calculated H ₂
50	1.03 10 ⁻⁸	3.9 10 ⁻⁹
100	1.34 10 ⁻⁸	7.8 10 ⁻⁹

Different authors have observed that γ -radiolysis of water in heterogeneous systems constituted of oxide and water induces an enhancement of H₂ production compared to pure water (Laverne et al. 2002, Laverne et al. 2003, Yamada et al. 2011). Different models have been proposed on the basis of energy transfer from the oxide surface to water by exited or secondary electrons. Yamada et al. (2011) have studied the effect of alumina on the enhancement of H₂ production by γ -radiolysis of pure water. They suggest that the adsorption of OH° radicals on the alumina surface limits its scavenging effect (R1 and R2) towards H₂. Therefore H₂ production increases.

Step 2 and Step 3: Corrosion under and after irradiation

After the plateau obtained at the beginning of the irradiation step, H₂ production rate increases with time, this increase being unchanged when irradiation is stopped (Fig. 23).

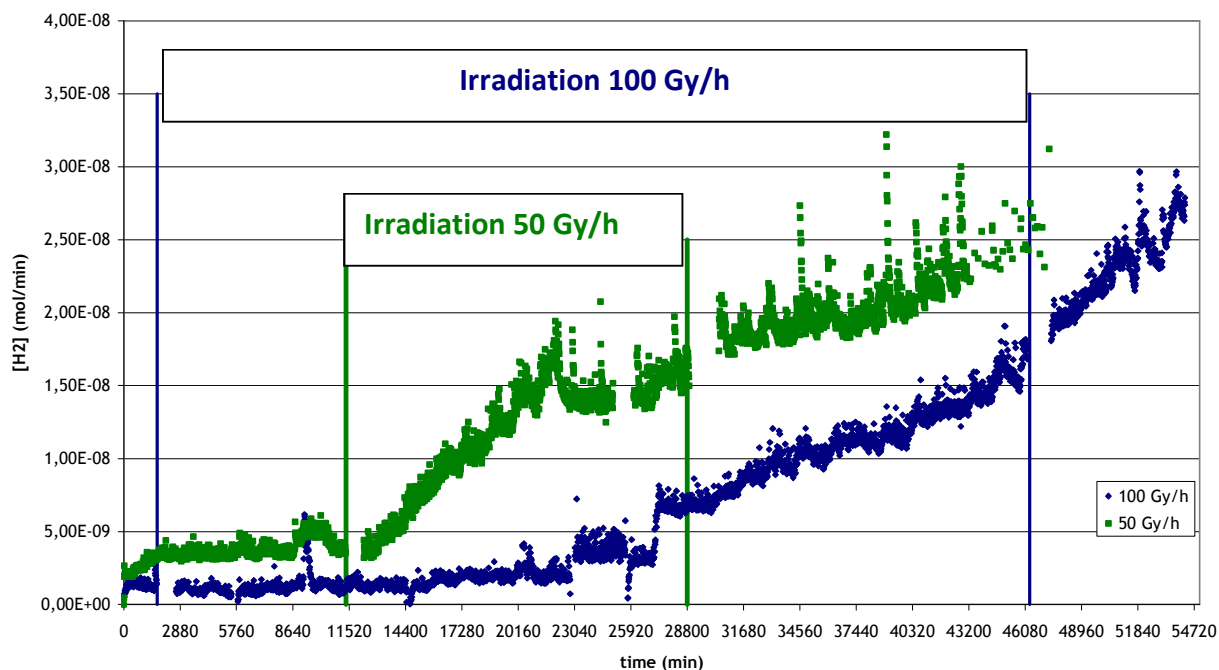


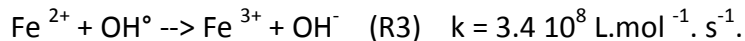
Fig. 23: Hydrogen production rate (mol/min) versus time (min) – Corrected from water radiolysis contribution.

Different mechanisms can induce this increase in H₂ production.

- Modifications of the composition of the solution

H₂ production rate by water radiolysis is constant at a constant dose rate but the decomposition rates are very sensitive to aqueous environments such as pH, temperature and

dissolved corrosion products (Yakabuskie et al. 2010). Joseph et al. (2008) have observed an increase in both H₂ and H₂O₂ production for pH higher than 10. Besides, Fe²⁺ is released in solution by iron corrosion. Under irradiation, radicals (OH°) are produced and can react with Fe²⁺ according to the following reaction (Fujita et al. 2010):



Considering the kinetic of this reaction (R3) which is very fast, the decomposition of H₂ through reaction R1 (see Table 7) cannot occur, Allen chain is disturbed and a large part of radiolytic products such as H₂ and H₂O₂ are preserved from recombination reactions.

However, in our experiments the increase in H₂ production continues when irradiation is stopped and considering the residence time of radicals (10⁻⁷ s), their influence on H₂ production should be limited to the irradiation phase. Therefore, it seems that this increase in hydrogen production is not only linked to a modification of water radiolysis processes.

- Modification of corrosion processes

Since water radiolysis produces both highly oxidizing (radicals and H₂O₂) and reducing species, it can control the redox conditions in our system and strongly influence the corrosion kinetics (Burns et al. 1983). For a potentially reactive material such as iron, the redox conditions are established by the interactions between reactive radiolysis products (H₂O₂, OH°), the steel surface and the corrosion products produced by these reactions. If radicals can induce transitory enhancement of corrosion, considering their residence times, their influence on iron corrosion is limited to the irradiation period. A molecular species like H₂O₂ is stable when irradiation is stopped and can also react with iron. However, when irradiation is stopped, this species is no more formed and its concentration should decrease with time according to oxidation reactions; thus the H₂ production rate should slow down. Considering the increase in H₂ production rate observed during several days in both experiments after irradiation was stopped, this hypothesis does not appear relevant.

- Modification of the corrosion layer structure

The chemical nature and morphology of surface oxide films and deposits are important parameters in controlling steel corrosion rates. Ionizing radiation may affect the semi-conducting properties of these passive films by altering the number and type of charge carriers, and induce a change in the corrosion rate. Irradiation has a major impact on the corrosion process by increasing the corrosion potential and therefore determining which oxide phase forms on the steel surface. Previous studies (Zhang et al. 2007, Daub et al. 2007) have found that the oxide formed in absence of radiation is mainly Fe₃O₄, while the oxide formed under irradiation has a mixed Fe₃O₄/γ-Fe₂O₃ structure. In the case of our experiments, the durations were too short to allow the formation of a detectable amount of passive films. Thus it is not possible to conclude on these phenomena on the basis of these two experiments.

2.4 CONCLUSIONS

At this stage of investigation, no consolidated explanation was found for the apparently continuous acceleration of hydrogen production rate observed in the irradiation experiments carried out at 100 and 50 Gy/h. Thus, additional studies are necessary:

- Longer experimental steps (corrosion before, under and after irradiation), in order to achieve steady-states (plateaus) for each of these steps and to obtain sufficiently thick corrosion layers for analyses at the end of the experiments (a whole experiment lasting at least several months);

- A better control of dissolved oxygen contents in de-aerated water, though difficult to reach, would be valuable. At least, speciation of iron in solution ($\text{Fe}^{2+}/\text{Fe}^{3+}$) at the end of the experiments would help to get information on the redox state of the system;
- Analysis of H_2O_2 at the end of experiments would provide information on its potential role on corrosion;
- Sensitivity experiments regarding the iron content in solution would also help assessing the role of this parameter in the H_2 generation by corrosion in a irradiating environment.

Besides, the development of a representative model of our experiment should allow a modelling of H_2 production (ChemSimul Software) and to test different hypotheses.

References

- Burns W.G., Marsh W.R., Walters W.S., The γ irradiation-enhanced corrosion of stainless and mild steels by water in the presence of air, argon and hydrogen, *Radiation Physics and Chemistry* 21 (1983) 259-279
- Brůha P., Pelech I., Czechoslovak patent no. 259785, Int. Cl. F 16 J 3/00, 1989.
- Daub K., Zhang X., Noel J.J., Wren J.C., Gamma-radiation-induced corrosion of carbon steel in neutral and mildly basic waters at 150°C, *Corrosion Science* 53 (2011) 11-16
- Delahay C.H, Alonso E.E., Soil heterogeneity and preferential paths for gas migration, *Engineering Geology* 64 (2002), 251-271
- Fujita N., Matsuura C., Saigo K., irradiation-enhanced corrosion of carbon steel in high temperature water – in view of a cell formation induced by γ -rays, *Radiation Physics and Chemistry* 58 (2000) 139-147
- Fujita N., Matsuura C., Saigo K., Radiation-induced preferential dissolution of specific planes of carbon steel in high-temperature water, *Radiation Physics and Chemistry* 60 (2001) 53-60
- Horseman S.T., Harrington J.F., Sellin P., Gas migration in clay barriers, *Engineering Geology* 54 (1999), 139 – 149
- Hunter F., Bole F., Heath T., Hoch R., Geochemical investigation of iron transport into bentonite as steel corrodes, SKB Technical Report, TR-07-09
- Joseph J. M., Choi B.S., Yakabuskie P.A., Wren J.C., A combined experimental and model analysis of the effect of pH and $O_2(aq)$ on γ -radiolytically produced H_2 and H_2O_2 , *Radiation Physics and Chemistry* 77 (2008) 1009-1020
- LaVerne J.A., Tandon L. H_2 production in the radiolysis of water on CeO_2 and ZrO_2 , *J. Phys. Chem.* 106 (2002) 380-386
- LaVerne J. A., Tonnics S.E., H_2 production in the radiolysis of aqueous SiO_2 suspensions and slurries *J. Phys. Chem. B.* 107 (2003) 7277-7280
- Yakabuskie P.A., Joseph J. M., Wren J.C., The effect of interfacial mass transfer on steady-state water radiolysis, *Radiation Physics and Chemistry* 79 (2010) 777-785
- Yamada R., Kumagai Y., Nagaishi R., Effect of alumina on the enhancement of hydrogen production and the reduction of hydrogen peroxide in the γ -radiolysis of pure water and 0.4 M H_2SO_4 aqueous solution, *International Journal of Hydrogen Energy* 36 (2011) 11646-11653